

January 2026
DESY 25-114

Very-High-Frequency Gravitational Waves from Multi-Monodromy Inflation

Guido D'Amico^{a,b,1}, Andrew A. Geraci^{c,2}, Nemanja Kaloper^{d,3} and
Alexander Westphal^{e,4}

^a*Department of Mathematical, Physical and Computer Sciences University of Parma,
43124 Parma, Italy*

^b*INFN Gruppo Collegato di Parma, 43124 Parma, Italy*

^c*Center for Fundamental Physics, Department of Physics and Astronomy
Northwestern University, Evanston, IL 60208, USA*

^d*QMAP, Department of Physics and Astronomy, University of California
Davis, CA 95616, USA*

^e*Deutsches Elektronen-Synchrotron DESY, Notkestr. 85,
22607 Hamburg, Germany*

ABSTRACT

We show that in multi-stage axion monodromy inflation an interruption near the end of the penultimate stage can lead to a spike in the gravitational wave background. These gravitational waves are in the frequency range and with an amplitude accessible to proposed terrestrial detectors such as the Einstein Telescope, Cosmic Explorer, and future Levitated Sensor Detector experiments.

¹guido.damico@unipr.it

²andrew.geraci@northwestern.edu

³kaloper@physics.ucdavis.edu

⁴alexander.westphal@desy.de

1 Introduction

Our Universe is big, old, and very smooth at the largest scales. The inflationary paradigm [1–3] is the leading candidate for explaining these facts in the framework of local causal theory of matter coupled to gravity. The idea was that at some early time and high energy, the universe underwent a stage of accelerated expansion, which blew it up quickly in a short period of time. To fit the observations of the late universe in the region which evolved from inside a small causally connected patch, the expansion should last about ~ 60 or so efolds. Typically, the models proposed to be behind such dynamics strive to accomplish it in one go, positing that there was a single such stage where all the required rapid expansion happened, after which the agent that drove the cosmic acceleration decayed into normal matter, allowing the expansion to slow down and smoothly connect to a radiation and matter dominated universe at late times. This decay process, or “reheating”, occurs at the end of inflation, and it involves complicated dynamics, but their signatures, if any, are at scales which today are typically contaminated by dynamics that came much later than inflation.

Realizing inflation in field theory is not so simple, however. Explaining the dynamics which yields almost-vacuum energy domination for a period of ~ 60 efolds and then disappears in the firework of particle production ending inflation requires nontrivial field dynamics, often needing scalar fields varying over (super-)Planckian ranges [4, 5]. Constructing meaningful models which can accommodate this is challenging in UV-complete frameworks, and at the very least it requires many ingredients with initial conditions which “conspire” to produce just the right environment (see, e.g. [6, 7]). Further, the direct tests of inflation are few and far between: the geometry of inflation is locally de Sitter space, which by its enhanced symmetry serves as a cosmic “amnesia tonic”, erasing the initial conditions, and, typically, the field dynamics during inflation, as codified in the cosmic no-hair theorem [8, 9]. Finally, many models are under pressure from the few observables which they produce, including the scalar power spectrum δ_S , the scalar spectral index n_S and the bounds on the primordial stochastic tensor background, parameterized by the tensor to scalar spectrum ratio r .

Yet, there is a simple variation of the conventional approach to inflation, which has been noted recently in [10], that can meet some of these challenges head-on. As an added bonus, this approach can produce additional testable signatures, naturally avoiding the obstacle of the no-hair theorem. The idea is to have inflation occur in stages, driven by multiple inflaton sectors which, while similar to each other, are separated by mass hierarchies (earlier discussions of various features of multi-stage inflation can be found in [11–20]). Such frameworks can be realized within the context of braneworlds, with multiple copies of inflatons arising from different branes, or from variants of the axiverse [21]. Some specific models were considered in [8, 9]. Here we will not delve into the model building details, instead focusing on the novel observational signatures they offer. In [22, 23] it was already noted that in models where the inflatons are axions which couple to dark $U(1)$ gauge fields, near the end of the inflationary stage dominated by one such field, there can be an exponentially enhanced production of $U(1)$ waves, which in turn quickly convert to primordial gravitational waves with an amplitude that greatly exceeds the usual stochastic gravity wave spectrum in a very narrow range of wavelengths. Such gravitational waves occur at scales much shorter than

the current horizon scale, and can be probed by an array of ongoing and planned surveys, such as NANOgrav, LISA, SKA and so on.

The stochastic gravitational wave backgrounds studied in [22, 23] concern gravitational waves with wavelengths of at least a few thousand kilometers, or with frequencies below 100 Hz. However, the interruptions during which they are formed occur at least 10 to 15 efolds before the end of inflation. This immediately suggests that if there are interruptions even later into inflation, during those even shorter wavelength gravitational waves can be induced. Indeed, a simple numerical estimate suggests that if the last 60 efolds of inflation began around the GUT scale, when the Hubble parameter is about 10^{14} GeV, and the reheating is very efficient producing the heat bath close to the GUT scale temperature, the scale factor of the subsequent decelerating universe would expand by a factor

$$\frac{a(\text{now})}{a(\text{reheating})} \sim \frac{T(\text{reheating})}{T(\text{now})} \sim \frac{10^{14} \text{ GeV}}{10^{-3} \text{ eV}} \sim 10^{26}, \quad (1)$$

i.e. by another ~ 60 efolds¹. Thus a gravitational wave formed at practically the end of this stage of inflation, frozen in with a wavelength $\lambda \sim 1/H(\text{inflation}) \sim 10^{-14} \text{ GeV}^{-1} \sim 10^{-26} \text{ mm}$ would stretch by FRW decelerated expansion to about $\lambda(\text{now}) \sim \text{mm}$ now. Such short gravitational waves could in principle be easily contaminated by the production of gravitational waves in later universe, and it could be very difficult to separate them out from the backgrounds induced by local physics.

However, given the argument above, it is clear that it does not take much to shift the wavelength up and consider gravitational waves which were produced somewhat earlier than the last efold of inflation. That would offer the possibility to search for such gravitational waves in the range of wavelengths where the contaminations induced by local physics happening in the late universe are small or absent. This is illustrated in Figure (1), which we adopted from [24], and which clearly and efficiently compiles the findings of the works [25–37], comparing the sensitivity of existing and planned experiments to the anticipated gravitational wave signals from a variety of sources. We direct the reader to [24] for a detailed interpretative discussion of Fig.1. Here we merely note that the signal which we consider may be powerful enough to exceed by orders of magnitude other sources, and may therefore win hands down over them in terms of possibilities for detection.

Indeed, once we restore the realistic cosmological parameters which match inflationary prediction within the context of multi-monodromy models of inflation, we find that if an interruption occurs few efolds (i.e. 6 to 10) before the end of the last 60 required to solve the flatness and homogeneity problems, the chiral gravitational waves produced by the inflaton decaying into a dark $U(1)$ which converts to gravitational waves have frequencies $f \sim 10^4 \text{ Hz} - 5 \times 10^5 \text{ Hz}$, which corresponds to wavelengths $\lambda \sim 30 \text{ km} - 600 \text{ m}$. This is in the domain that could be explored with terrestrial experiments such as Einstein Telescope or Cosmic Explorer ($\sim \mathcal{O}(10 \text{ km})$) or extended versions of the Levitated Sensor Detector

¹In this argument we are assuming that the interrupted universes are radiation-dominated, following a very successful reheating after each interruption. This is for illustrative purposes only. If e.g. the interrupted epochs were matter-dominated the same argument would persist, the only change being some numerical modifications of the relationship between relic wavelengths, cosmological parameters and the efold where the interruption occurs.

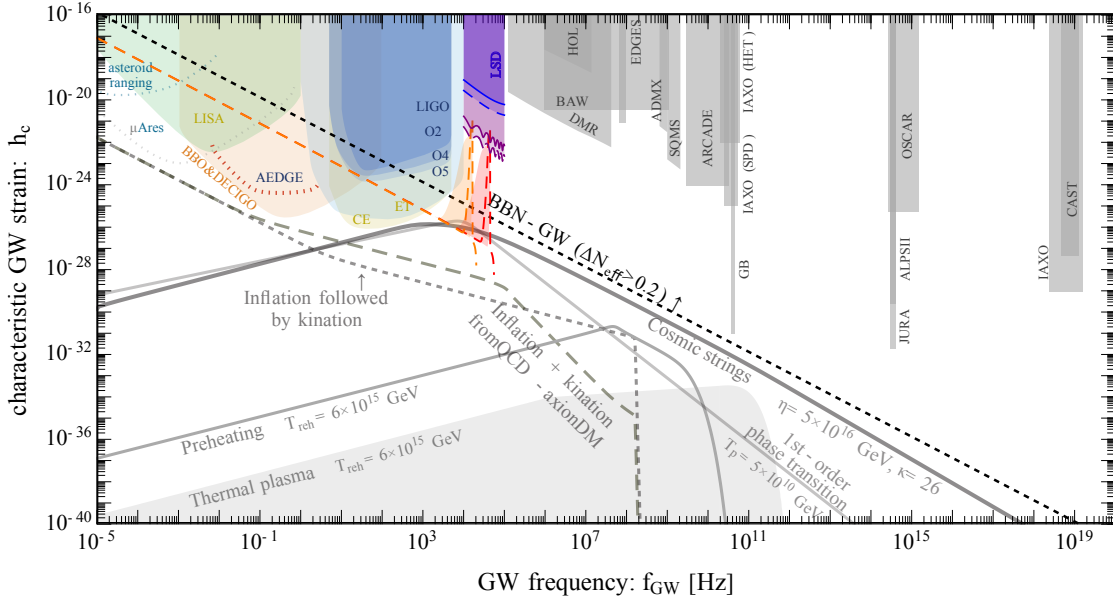


Figure 1: Gravitational wave strain as a function of frequency from different sources discussed in the literature, such as cosmic strings, preheating after inflation, the hot thermal post-big bang plasma, etc. The bright red colored spikes near the center of the image are the signals derived in this paper. Clearly, if they were present in our universe they would dominate over other sources.

($\sim \mathcal{O}(100 \text{ m})$). It turns out that the amplitude of these gravitational waves is right around the detection threshold of these instruments. This evades the bounds on the gravitational wave power depicted in Fig.1, specifically both the limits coming from Big Bang Nucleosynthesis (BBN) and from the consideration of cosmic string sources, because our signal has a very narrow frequency range, and therefore the total power of these gravitational waves, indicated by the area below the red spikes in Fig.1, is easily much smaller than the area below the BBN limiting curve and the cosmic strings curve even when the red spike is as many as $\sim \mathcal{O}(10)$ orders of magnitude larger.

This remarkable happenstance therefore offers a chance to search for signatures of inflationary cosmology, which while model dependent, follow from arguably realistic models of inflation from the point of view of UV physics. Combined with more interruptions, and corresponding gravitational waves sourced with larger wavelengths, this offers a remarkable opportunity for searching for new physics from inflation with gravitational wave detectors. In our view this exciting possibility deserves serious and detailed exploration.

2 Multi-monodromy inflation and the “characteristic” spectrum of GW signals

Axions are attractive candidates for driving cosmological slow-roll inflation, both from the bottom-up EFT point as well as within string theory. The reason is the discrete shift

symmetry and the dual formulation gauge symmetry, which good axions enjoy, which in turn constrains corrections to the axion scalar potential to arise in powers of those operators involved in generating the leading-order axion potential in the first place. As this removes the appearance of arbitrary just M_P -suppressed monomial terms, the so-called eta problem is absent for axion inflation models.

The scalar potential for axion inflation can arise as a manifestly periodic potential from non-perturbative quantum corrections breaking the continuous shift symmetry down to a discrete subgroup. Or the axion can acquire an infinite set of individually non-periodic power-law scalar potentials from axion monodromy [6, 38–40]. This infinite set of branches with their minima separated by $2\pi f$ realizes the discrete shift symmetry as a property of the full branch system of scalar potentials, even though the individual branch breaks the shift symmetry completely. Here, f denotes the axion decay constant of the axion arising from its kinetic term, which in turn sets the periodicity scale $2\pi f$ of the non-perturbative quantum corrections.

We can get this core mechanism of axion monodromy both for the KK zero mode axions arising from higher p -form gauge fields of string theory compactifications in the presence of either branes or higher-dimensional quantized q -form field strengths, and from the unique 4D EFT description of a massive axion arising from mixing a pseudo-scalar with a non-dynamical but vacuum energy changing 4-form field strength. As the protection² of the branch scalar potentials from most quantum corrections is much more transparent from the underlying gauge symmetries governing the 4D effective massive 3-form gauge theory [6, 39] (see also [42] for important precursor work), we will largely stick with this 4D effective description

$$\frac{\mathcal{L}}{\sqrt{-g}} = -F_{\mu\nu\rho\sigma}^2 - (\partial\phi)^2 - m\phi\epsilon_{\mu\nu\rho\sigma}F^{\mu\nu\rho\sigma} . \quad (2)$$

Carefully integrating out the 4-form field strength $F_{\mu\nu\rho\sigma} = \partial_{[\mu}A_{\nu\rho\sigma]}$ shows the axion ϕ acquiring an infinite set of branches of quadratic scalar potentials $\sim m^2\phi^2$.

A generic feature of axion monodromy inflation is the dynamics of flattening - the branch scalar potential tends to flatten out below the tree-level ϕ^2 -behavior when ϕ is displaced by more than a distance $\mu = \mathcal{O}(0.1 - 1) M_P$ from the branch minimum. This flattening is already contained in the 4D effective flux monodromy description [6, 39] once higher gauge-invariant operators are included. We will assume scaling relationships between the Wilson coefficients of these operators such that the whole series resums into a flattened power-law form visible in the existing simple string models of axion monodromy inflation. Given this background story, the effective scalar potential for an axion from axion potential on each branch takes the form

$$V(\phi) = M^4 \left[\left(1 + \frac{\phi^2}{\mu^2} \right)^{p/2} - 1 \right] . \quad (3)$$

Here the scale M is ultimately determined by fitting the CMB temperature anisotropy amplitude. For the asymptotic power p of the scalar potential $V \sim \phi^p$, $\phi \rightarrow \infty$ we take

²The gauge symmetries do not completely tame all UV dangers since the gauge field mass might be UV sensitive, as in e.g. hierarchy problem (we ignore the cosmological constant problem). We assume that some mechanism in the UV completion of the theory fixes it to be sufficiently small, and then the gauge symmetries maintain control of other operators [41].

guidance from the known top-down string examples which suggest $0.1 \lesssim p < 1$. As long as the axion has canonically normalized 2-derivative kinetic term, this largely fixes the CMB observable predictions to $n_s > 0.975$ and $0.02 < r < 0.08$, which is too blue an n_s given the current constraints from data [22, 43, 44]. Axion monodromy inflation is a large-field model of inflation, and we see this here for the range of p as well, where 60 efolds of inflation correspond to $\mathcal{O}(5 - 10) M_P$ of field range traversed.

Clearly, the setup with a single axion with a 2-derivative kinetic term and the type of flattening motivated from string theory examples is under pressure from the data. We alleviate this by widening our view:

- The gauge symmetries governing the 4D EFT of axion monodromy allow for higher-derivative kinetic terms of the axion. Examples constructed from adding a few such terms perturbatively as motivated from bulk α' -corrections in string theory, or by adding an infinite series of such terms motivated from DBI action of D-branes, show that these higher-derivative terms will lower r by decreasing the speed of sound c_s of the curvature perturbation at the price of increasing the amount of equilateral non-Gaussianity f_{NL} . From the existing CMB bounds on f_{NL} , we infer that higher-derivative axion kinetic terms can suppress the lower bound on r to about $r \gtrsim 0.006$.
- A look at the structure of the six or seven extra dimensions used for compactifying string theory to 4D shows us that many choices have a large number of non-trivial subspaces ('cycles') within the compact extra dimensions. Together with the existence of higher p -form gauge potentials in string theory this leads to typical string compactifications having many axions as KK zero modes of those gauge potentials – a string ‘axiverse’.

Hence, there is no reason to assume that the observable 60 efolds of inflation have to come from continuous slow-roll of a single axion. Instead, several axions with each of them having a potential from monodromy may share the work [10, 22, 23].

If, as will be typical without special arrangements, the scalar potential for each axion will have a somewhat different overall scale, inflation will then proceed in several stages. Assume a small number N of axions are displaced from their respective minima by several M_P . The heaviest axion will initial slow-roll, with the lighter axions being in very deep slow-roll essentially frozen in their smaller potentials. Once the heaviest axion rolls off into its minimum, it will break slow-roll for a short period of 2-3 efolds of red-shifting matter domination until the next-lighter axion’s potential energy starts driving slow-roll inflation again once beginning to dominate. The story repeats with each subsequent lighter and displaced axion, leading to ‘roller-coaster’ monodromy inflation.

For the sake of simplicity, we will assume only 2 axions participating (see Fig.2)

$$V(\phi_1, \phi_2) = M_1^4 \left[\left(1 + \frac{\phi_1^2}{\mu_1^2} \right)^{p_1/2} - 1 \right] + M_2^4 \left[\left(1 + \frac{\phi_2^2}{\mu_2^2} \right)^{p_2/2} - 1 \right] . \quad (4)$$

The crucial point is that the ~ 7 observable efolds of the CMB will arise only from the part of inflation driven by the heavier axion. Hence, the CMB properties will be determined by the heavier axion slow-rolling only for $\Delta N_e < 60$ efolds. The other needed $60 - \Delta N_e$ efolds

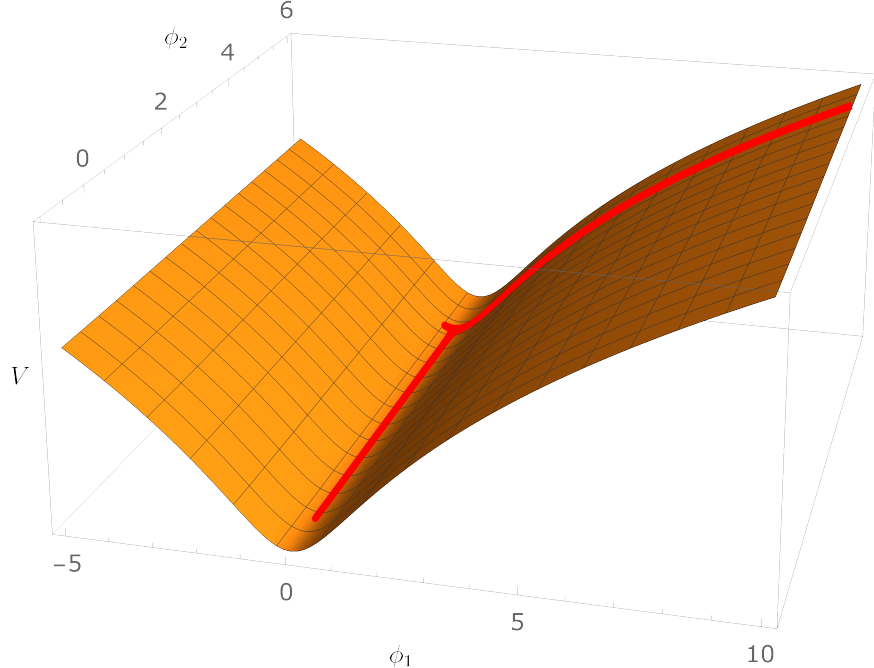


Figure 2: Two-field potential $V = V(\phi_1, \phi_2)$ for the model in eq. (2). Here $M_2/M_1 = 0.1$, $p_1 = 2/5$, $p_2 = 1$, $\mu_1 = \mu_2 = \mathcal{O}(1) M_P$. The red curve depicts a typical two-stage inflationary trajectory, where the field ϕ_1 slow-rolls down the slope first and then oscillates while decaying near the bottom of the valley. Finally, ϕ_2 starts to move along the valley.

are supplied after the break by the 2nd lighter axion. Since for large-field inflation models the CMB spectral index scales as $n_s = 1 - \#/\Delta N_e$, we can have axion monodromy inflation with a good n_s by doing double monodromy with two axions and placing the break at about 35 efolds before the end of inflation.

Incidentally, splitting up the full 60 efolds of slow-roll into several epochs driven by different axions has the effect of reducing the individual axion field displacement below the $\mathcal{O}(5 - 10) M_P$ needed for a single axion doing all the work. Given recent discussions in the literature about potential control issues for large trans-Planckian displacements of (pseudo)scalars due to the appearance of new states entering the original EFT, this may turn out to be a benefit.

For our purpose, the most interesting feature of this mechanism of rollercoaster axion monodromy is the possibility of one or several of the axions driving inflation to couple to a dark U(1) gauge field

$$\mathcal{L}_{\text{int}} = \sqrt{-g} \frac{\phi_i}{4f_{\phi_i}} F_{i\mu\nu} \tilde{F}_i^{\mu\nu} . \quad (5)$$

Here, we used again input from string constructions which seem to suggest that a given axion couples to at most a handful of different gauge fields, and often to just one (if at all – often the U(1) gauge fields get Stueckelberg lifted and thus very massive). The f_{ϕ_i} denote the axion decay constants. For string axions, the decay constants arise from compactification of the extra dimensions and depend on inverse powers of the radii. As we assume these to be

larger than the string scale, the decay constants are sub-Planckian.

The above coupling to gauge fields is interesting. Assume that the heavier of our 2 axions driving the 1st stage of inflation is coupled to a dark $U(1)$ gauge field this way. Provided f_{ϕ_1} is small enough, the increasing speed of ϕ_1 towards the end of its stage of inflation is known to generate a tachyonic-like instability for one of the 2 helicity eigenstates of the $U(1)$ gauge field (see the appendix of [45]). This leads to the generation of chiral gauge field quanta and quite drastic exponential production of this gauge field mode [46, 47]. The maximum production level is bounded by the axion inflaton kinetic energy close to its slow-roll breaking exit point.

Once these chiral gauge field quanta have been sourced, they in turn source a secondary peaked spectrum of stochastic gravitational waves [48–50]. Their contribution to the energy density of the universe is given by

$$\Omega_{GW} \equiv \frac{\Omega_{r,0}}{24} \Delta_T^2 \simeq \frac{\Omega_{r,0}}{12} \left(\frac{H}{\pi M_P} \right)^2 \left(1 + 4.3 \cdot 10^{-7} \frac{H^2}{M_P^2 \xi^6} e^{4\pi\xi} \right) . \quad (6)$$

Here, we denote with $\Omega_{r,0} = 8.6 \cdot 10^{-5}$ the present-day radiation density parameter. The quantity $\xi = \dot{\phi}_1/(2Hf_{\phi_1})$ controls the efficiency of the gauge field production and thus the strength of the overall effect. Strong gauge field production requires an axion decay small enough so that $\xi \gtrsim 3$ (see e.g. [51, 52] for non-perturbative numerical treatments of the gauge field production and its backreaction on the inflationary dynamics).

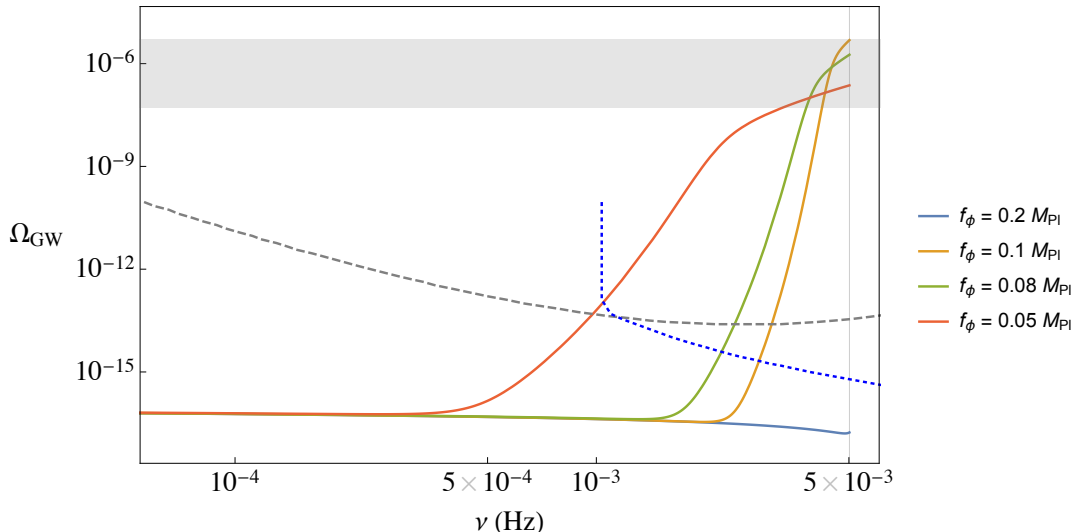


Figure 3: Abundance of gravitational waves as a function of frequency, setting $N_{CMB} = \Delta N_e = 35$. Dashed grey: the sensitivity of LISA. Dotted blue: the sensitivity of Big Bang Observer (BBO). The example given here uses $M_1^4 = 2 \times 10^{-9} M_P^4$, $\mu_1 = M_P$, $p_1 = 0.2$. We scan f_{ϕ_1} over the values shown in the legend.

This is the signal we are after. As the GW production traces the gauge field production, its peak frequency is determined by the number of efolds before the end of inflation when the first axion ends its inflationary stage and exits into the 2-3 efolds lasting break of oscillations

providing matter domination. Using the relation between efold number and scale factor which in turn relates physical and comoving frequency $\nu = k/(2\pi)$, we can express the frequency in terms of the number of efolds before the end of inflation:

$$N = N_{CMB} + \ln \frac{k_{CMB}}{0.002 \text{ Mpc}^{-1}} - 44.9 - \ln \frac{\nu}{10^2 \text{ Hz}} , \quad (7)$$

where N , N_{CMB} are measured backwards from the moment of the end of inflation, when the signal peaks, and we fix N_{CMB} to be the time when CMB scales left the Hubble radius. Then $k_{CMB} = 0.002 \text{ Mpc}^{-1}$ is the pivot scale.

We see that by choosing appropriate initial field values ϕ_{i0} for our two axions, we can arrange the efold time ΔN_e of the break between the two stages of inflation. This in turn determines the frequency of the GW peak sourced by the gauge field production of the first heavier axion: if the first stage of inflation driven by ϕ_1 lasts ΔN_e efolds before the break, then the observed CMB scales arise at $N_{CMB} = \Delta N_e$ efolds before the end of the first stage. An example of the expected spectrum for $\Delta N_e = 35$ and different f_{ϕ_1} is in Fig.3. If we place the break at about $\Delta N_e = 50 - 51$ the resulting frequency range of the GW peak will fall into the 10 kHz range of our levitating-sensor based detector.

3 The axion GW signal

We now look in more detail at the properties of the burst of primordial gravitational waves produced by double monodromy inflation coupled to a dark $U(1)$ gauge field. This stochastic GW signal is peaked at some frequency f_p , which can vary (at production) from about few nHz to about 10 MHz, and with a width $\Delta f_p \simeq \frac{1}{10} f_p$. This is a rough estimate, but it should be correct by order of magnitude.

In more detail, the signal can peak at different frequencies, depending on the number of efolds when the stage of inflation ends by decay into gauge fields. Seeing such gravitational waves would show the existence of a dark $U(1)$ gauge sector, which is an amazing perspective.

The range 10 kHz – 300 kHz corresponds to a range of efolds $N_{CMB} = 50 - 52$ measured from the moment when the CMB scales left the Hubble radius, as seen in Fig.4. Here we have plotted a few different N_{CMB} , with a fixed axion coupling, spanning the range of frequencies to which the Levitated Sensor Detector is sensitive.

The grey area is an uncertainty, due to neglecting backreaction effects. But this shows that we can reach the maximum value $\Omega_{GWh}^2 \sim 5.7 \times 10^{-6} \Delta N_{\text{eff}} \simeq 2 \times 10^{-6}$ allowed by bounds on ΔN_{eff} . For the purpose of detection, we should determine the frequency width of the signal. The $\Delta f/f$ is practically the same for all peaks, so we plot just one in Fig.5, stopping at the ΔN_{eff} bound. The peaks are narrow, but not so much. From Fig.5 we see that the width in frequency can be estimated as $\Delta f/f \simeq 0.1$. With a full treatment, this may be larger, possibly up to $\Delta f/f \simeq 0.2$ which is what we estimate if we take the plot up to the full peak.

We can now look at the strain h , which is the quantity of interest in detection experiments. Here we make the assumption that our cosmological signal is stochastic, in the sense that the amplitudes $h(f)$ are random variables, of which we can predict correlators. For estimates of the signals potentially observable in experiments, we make the following assumptions:

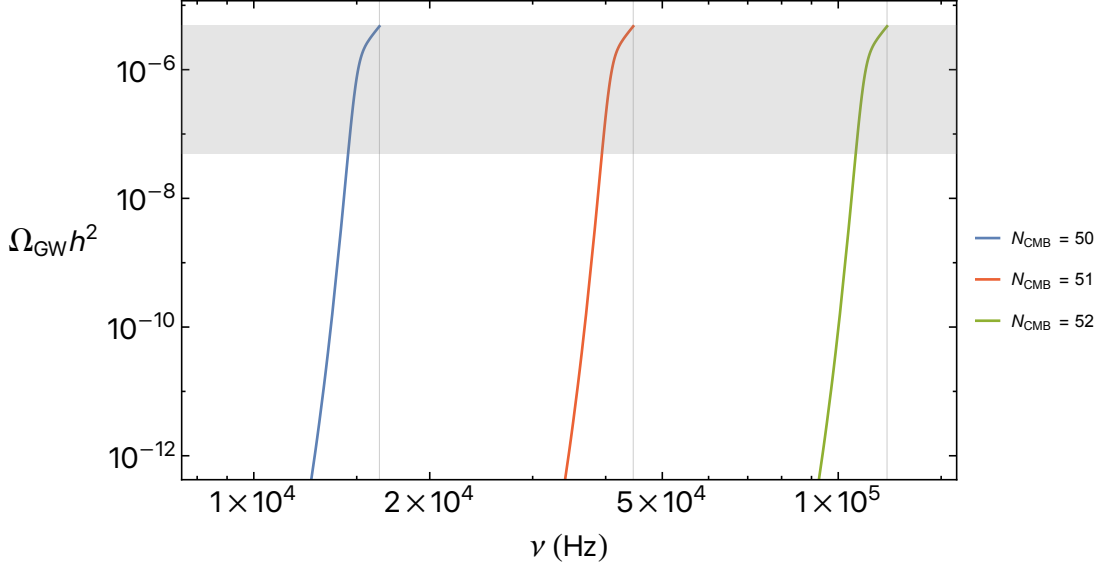


Figure 4: Abundance of gravitational waves as a function of frequency for different values of N_{CMB} , corresponding to the range of frequencies probed by the Levitated Sensor Detector.

- Stationarity (time-translation invariance). This implies that $\langle h^*(f)h(f') \rangle$ is proportional to $\delta_D(f - f')$.
- Gaussianity. This means that the signal is characterized only by the 2-point function (assuming zero mean).
- Isotropic and not polarized background. This implies that we'll suppress angular and polarization information.

The signal can be modeled by defining the spectral density of the background

$$\langle h^*(f)h(f') \rangle = \delta_D(f - f') \frac{1}{2} S_h(f). \quad (8)$$

What we predict is the energy density in GW, defined by

$$\rho_{GW} = \Omega_{GW} \frac{3c^2 H_0^2}{8\pi G} = \frac{c^2}{32\pi G} \langle \dot{h}_{ij} \dot{h}^{ij} \rangle. \quad (9)$$

It is now convenient to write Ω_{GW} as an integral over log frequencies. Given the definition of $S_h(f)$, we get

$$\Omega_{GW} = \frac{1}{3H_0^2} \int_0^\infty d \ln f f (2\pi f)^2 S_h(f), \quad (10)$$

where a factor of 4 comes from the sum over polarizations. It is common to now define a dimensionless “spectral density” $\Omega_{GW}(f)$ by the equation

$$\Omega_{GW} = \int_0^\infty d \ln f \Omega_{GW}(f). \quad (11)$$

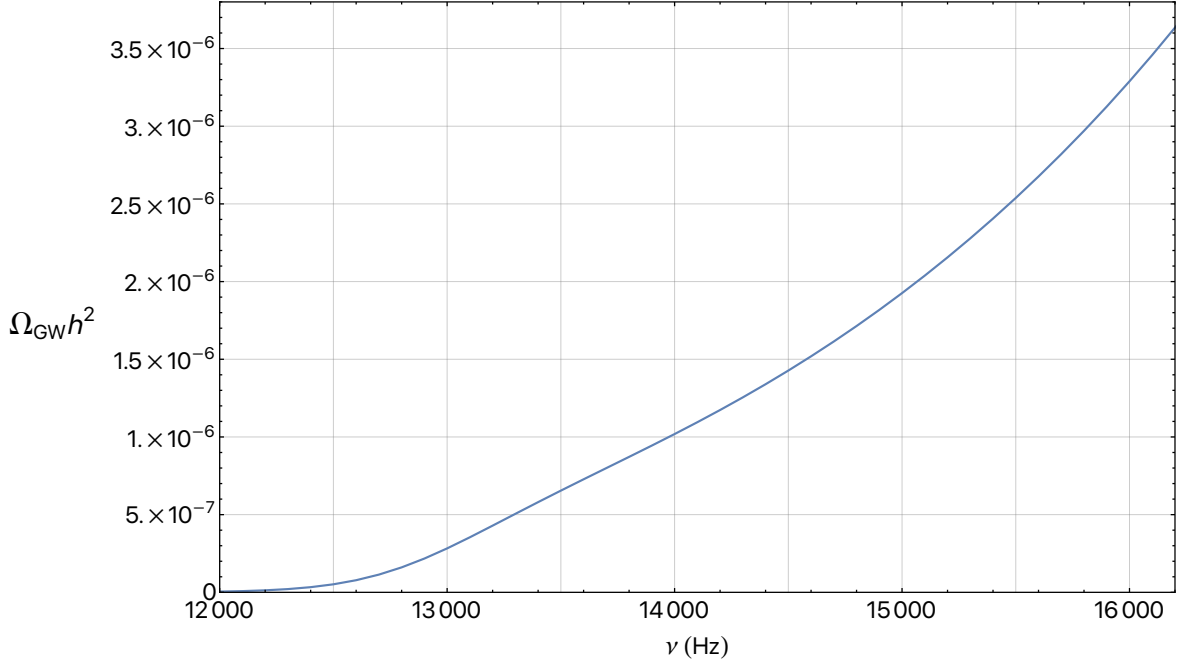


Figure 5: High-resolution plot of the rising edge of the gravitational wave peak as a function of frequency for $N_{CMB} = 50$ corresponding to a ~ 15 kHz range signal.

The strain spectral density S_h is related to the dimensionless $\Omega_{GW}(f)$ (in frequency band f) by

$$\Omega_{GW}(f) = \frac{4\pi^2}{3H_0^2} f^3 S_h(f). \quad (12)$$

The S_h has dimensions of inverse frequency, and it has a characteristic $1/f^3$ behavior for the scale invariant case in which $\Omega_{GW}(f)$ does not depend on frequency. The quantity that commonly appears in the sensitivity plots is the strain $h(f) = \sqrt{S_h(f)}$, which has units of $\text{Hz}^{-1/2}$, and is given by

$$h = \left(\frac{3H_0^2}{4\pi^2} f^{-3} \Omega_{GW}(f) \right)^{1/2}. \quad (13)$$

In sensitivity plots, as in our Fig.6, it is common to plot a curve representing the bound on ΔN_{eff} from BBN or CMB observations. As mentioned in the introduction, it is important to note that such a curve represents the bound only in the case of a scale-invariant spectral density. For our case, in which the $\Omega_{GW}(f)$ quantity is strongly peaked around a single frequency, the signal can cross the scale-invariant bound curve. In fact, the measurements of ΔN_{eff} translate in a bound on the full integral [53]:

$$\int_{f_{\text{BBN}}}^{\infty} d \ln f \Omega_{GW}(f) < 1.2 \times 10^{-5} \Delta N_{\text{eff}}, \quad (14)$$

where $f_{\text{BBN}} \simeq 10^{-12} \text{ Hz}$ is the frequency corresponding to the horizon size at BBN, and $\Delta N_{\text{eff}} \lesssim 0.12$ [54, 55]. We have checked that our signal satisfies the bound.

4 Estimating the sensitivity for the Levitated Sensor Detector

The ground based laser interferometry gravitational observatories have attained a remarkable strain sensitivity to gravitational waves at frequencies below 10 kHz [56]. At higher frequencies, the sensitivity of such instruments is limited by photon shot noise. Although advanced quantum sensing techniques such as squeezing can provide improvements for certain regimes of operation [57], in this higher frequency band, levitated optomechanical sensors provide a route towards substantially improved sensitivity [58–60]. In these instruments, a dielectric particle is suspended in an optical cavity and acts as a high-Q mechanical oscillator, with the gradient in the laser intensity along the optical standing wave providing the restoring force trapping the particle at an anti-node of the cavity field. Due to the high mechanical Q and relatively large displacement when driven on resonance, photon shot noise is not the dominant mechanism that limits the sensitivity. Rather the sensitivity is limited by thermal noise in the motion of the particle, or in the extreme high vacuum limit by the radiation pressure shot noise associated with photon recoil heating of trap laser photons [59, 61]. While the photon shot noise limited sensitivity of interferometer detectors such as LIGO becomes worse at higher frequency, the thermal noise limited sensitivity tends to improve, making the levitated sensor approach favorable with respect to an optical interferometer. The Levitated Sensor Detector currently under construction at Northwestern is a 1-meter prototype instrument intended to explore this technology. The design sensitivity of the pilot instrument and future 10-meter or 100-meter long versions of the detector has been described in Ref. [59]. For the longest version considered previously, the strain sensitivity is of order $\sim 10^{-23}/\sqrt{\text{Hz}}$, and would not be sufficient to detect the predicted signals within an observing time of 10^8 seconds.

However, it is possible to consider extending the length of such as setup to the 10 kilometer scale of upcoming next generation observatories such as Einstein Telescope or Cosmic Explorer. One challenge of realizing this for a levitated optomechanics setup has to do with the need for a small mode waist. The setup involves a Michelson interferometer configuration with Fabry-Pérot arms of length L as described in Ref. [59], where a dielectric disk-shaped object is suspended at an anti-node of the standing wave inside each Fabry-Pérot arm, where the optical restoring force results in a trapping frequency ω_0 . A second laser can be used to read out the position of the object as well as cool it along the cavity axes, as described for a similar setup in Ref. [58]. A passing GW with frequency Ω_{gw} imparts a force on the trapped particle [58], which is resonantly excited when $\omega_0 = \Omega_{\text{gw}}$. Unlike a resonant-bar detector, ω_0 is widely tunable with laser intensity. The second cavity arm permits rejection of common mode noise, for example from technical laser noise or vibration.

The minimum detectable strain h_{limit} for a particle of mass M with center-of-mass temperature T_{CM} is approximately [58]

$$h_{\text{limit}} = \frac{4}{\omega_0^2 L} \sqrt{\frac{k_B T_{\text{CM}} \gamma_g b}{M}} \left[1 + \frac{\gamma_{\text{sc}}}{N_i \gamma_g} \right] H(\omega_0), \quad (15)$$

where the cavity response function $H(\omega) = \sqrt{1 + (2\mathcal{F}/\pi)^2 \sin^2(\omega L/c)}$ for a cavity with finesse \mathcal{F} and corresponding linewidth $\kappa = \pi c/L\mathcal{F}$. Here $N_i = k_B T_{\text{CM}}/\hbar\omega_0$ is the mean

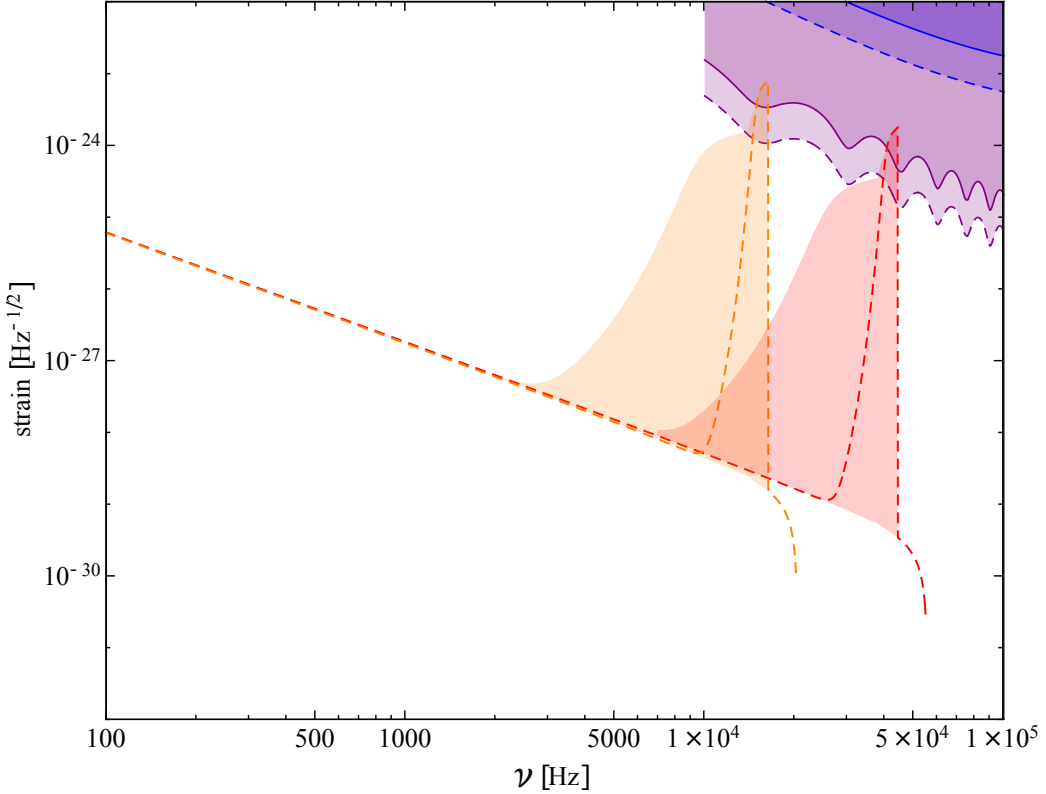


Figure 6: Estimated gravitational wave strain as a function of frequency, setting for different $N_{\text{CMB}} = 50, 51$ (orange, red). The dashed curve corresponds to $f_\phi = 0.1 M_{Pl}$ and the shaded region represents an envelope with f_ϕ ranging from 0.05 to 0.15 M_{Pl} . Also shown are the sensitivity estimates of the Levitated Sensor Detector for two different lengths $L = 100$ m (blue) and $L = 10$ km (purple) for two different masses of the levitated particle, corresponding to the system studied in Ref. [59] (solid) as well as three times larger mass (dashed).

initial phonon occupation number of the center-of-mass motion. $\gamma_g = \frac{32P}{\pi\bar{v}\rho t}$ is the gas damping rate at pressure P with mean gas speed \bar{v} for a disc of thickness t and density ρ , and b is the bandwidth. The photon recoil heating rate [58, 62] $\gamma_{sc} = \frac{V_c\lambda\omega_0}{4L} \frac{1}{\int dV(\epsilon-1)} \frac{1}{\mathcal{F}_{\text{disc}}}$ is inversely proportional to the disc-limited finesse $\mathcal{F}_{\text{disc}}$, i.e. (2π) divided by the fraction of photons scattered by the disc outside the cavity mode. The integral is performed over the extent of the suspended particle. Here V_c is the cavity mode volume [58], ϵ is the particle dielectric constant, and λ is the trapping laser wavelength.

For the application of GW detection, using high-mass, high-trap-frequency, disc- or plate-like microparticles is ideal for achieving maximal sensitivity with this technique. Recent experimental work has demonstrated optical trapping of high-aspect-ratio hexagonal prisms with a 20 micron-scale radius [61]. The prisms are trapped in vacuum using an optical standing wave, with the normal vector to their face oriented along the beam propagation direction, yielding much higher trapping frequencies than those typically achieved with microspheres of similar mass. This plate-like geometry is planned to be used in high frequency gravita-

Parameter	Units	$L = 100$ m	$L = 100$ m	$L = 10$ km	$L = 10$ km
$\omega_0/2\pi$	kHz	10	100	10	100
I_0	W/m^2	2.2×10^8	2.2×10^{10}	2.2×10^8	2.2×10^{10}
\mathcal{F}	—	10	10	3	3
$N_i\gamma_g$	Hz	0.54	0.054	0.54	0.054
γ_{sc}	Hz	0.004	0.041	0.004	0.041
h_{\min}	$1/\sqrt{\text{Hz}}$	7.9×10^{-22}	1.7×10^{-23}	1.5×10^{-23}	2.0×10^{-25}

Table 1: Experimental parameters for trapping of a $75\ \mu\text{m}$ radius stack with $14.58\ \mu\text{m}$ thick SiO_2 spacer (corresponding to $j = 28$) and quarter-wave $110\ \text{nm}$ thick Si endcaps in a cavity of length L at $P = 10^{-11}$ Torr and room temperature. I_0 is the peak laser intensity striking the disc and $h_{\min} = h_{\text{limit}}/\sqrt{b}$ is the strain sensitivity where b is the measurement bandwidth.

Parameter	Units	$L = 100$ m	$L = 100$ m	$L = 10$ km	$L = 10$ km
$\omega_0/2\pi$	kHz	10	100	10	100
I_0	W/m^2	2.2×10^8	2.2×10^{10}	2.2×10^8	2.2×10^{10}
\mathcal{F}	—	10	10	3	3
$N_i\gamma_g$	Hz	0.17	0.017	0.17	0.017
γ_{sc}	Hz	0.0013	0.013	0.0013	0.013
h_{\min}	$1/\sqrt{\text{Hz}}$	2.5×10^{-22}	5.5×10^{-24}	4.8×10^{-24}	6.4×10^{-26}

Table 2: Experimental parameters for trapping of a $75\ \mu\text{m}$ radius stack with $45.82\ \mu\text{m}$ thick SiO_2 spacer (corresponding to $j = 88$) and quarter-wave $110\ \text{nm}$ thick Si endcaps in a cavity of length L at $P = 10^{-11}$ Torr and room temperature. I_0 is the peak laser intensity striking the disc and $h_{\min} = h_{\text{limit}}/\sqrt{b}$ is the strain sensitivity where b is the measurement bandwidth.

tional wave searches in the Levitated Sensor Detector, currently under construction [59]. We consider a setup with parameters as described in Tables 4 and 4, corresponding to different cavity lengths, finesse, and masses for the levitated dielectric stack. Relative to the setup described in prior work [59], the longer (10 km) configuration would need an additional lens to focus the beam near the input mirror of each arm cavity, to provide sufficient transverse restoring force to support the particle against the earth’s gravity. We assume that the modest cavity finesse shown in Tables 4 and 4 can be achieved in the presence of such a lens and that with sufficient vibration isolation and use of low-loss materials, the contribution of the lens to the noise budget of the system can be made comparable to the Fabry-Pérot end mirrors.

In Fig.6, we illustrate the sensitivity for an integration time of 10^8 seconds for two particular cases of a signal corresponding $N_{\text{CMB}} = 50, 51$. Here we illustrate one particular value of $f_\phi = 0.1M_{Pl}$ as a dotted curve and show an envelope obtained by varying the value from $f_\phi = 0.05M_{Pl}$ to $f_\phi = 0.15M_{Pl}$. This envelope provides us with a rough estimate of the ‘theory error’ encapsulating a UV theory motivated range of the otherwise unknown value of the axion decay constant f_ϕ . The cavity response function can be approximated

as $H(\omega) \approx \sqrt{1 + 4\omega^2/\kappa^2}$ for a sufficiently short cavity, e.g. valid for the blue solid and dashed curves shown in Fig.6 for the 100 m long cavity. For the longer 10 km arm cavity we consider, the oscillations of the sine function are visible in the estimated sensitivity curve.

Considerations for multiple detectors. For a single detector, the presence of a stochastic GW background signal would manifest essentially as excess noise in the relevant frequency band for example as shown in Fig.6. Defining a factor F that takes into account the angular efficiency of the detector, the signal-to noise ratio, for each frequency f is

$$\left(\frac{S}{N}\right)^2(f) = F \frac{S_h(f)}{S_n(f)} \quad (16)$$

where $S_n(f)$ is the noise spectral density. Supposing the noise spectrum is essentially flat over the bandwidth of the signal, we can consider integrating over a frequency window of $\Delta f \lesssim \Delta f_p$, corresponding to an observational time $T \gtrsim \frac{1}{\Delta f_p}$. Using the frequencies in the plot, for the smallest $f_p \simeq 10$ kHz, we require $T \gtrsim \frac{1}{\Delta f_p} \simeq 10^{-3}$ s. Then for averaging times up to 10^{-3} the signal is essentially phase coherent whereas the noise is incoherent e.g. for a thermal noise background, so that the signal to noise ratio improves, scaling as $T^{1/2}$. For longer averaging times, e.g. such as the 10^8 s considered in Fig.6, the phase of the signal varies as the time duration exceeds the coherence time, and the scaling of the improvement with averaging time is reduced to $T^{1/4}$, as is typically the case for detection of other stochastic strain-related signals such as that resulting from dilatonic ultralight dark matter [63].

When we have two detectors, we can try and correlate the outputs to separate the (correlated) signal from the noise, in particular for two detectors that are separated by a distance Δx small compared to the gravitational wave wavelength, i.e. $\Delta x \lesssim \frac{c}{2\pi f}$. To estimate this range, take now the largest frequencies of the plot, $f_{\max} \simeq 100$ kHz, this requires

$$\Delta x \lesssim \frac{3 \times 10^8}{2\pi \times 10^5} \text{ m} \simeq 400 \text{ m}, \quad (17)$$

which is reasonably achievable for 100 m long detector arms. In this regime we expect a factor of $\sqrt{2}$ improvement in the sensitivity due to the correlated signal, which scales as \sqrt{N} for N instruments. At 10 kHz this distance increases to 4 km. For the 10 km baseline taken for the largest scale instrument we consider, this length is larger than the gravitational wave wavelengths being considered.

5 Summary

In this paper we have considered a class of inflationary scenarios in which accelerated expansion proceeds in multiple stages, driven by several inflaton sectors separated by mass hierarchies. Rather than realizing the required ~ 60 efolds of inflation in a single continuous phase, inflation is intermittently interrupted as the dominant inflaton sector changes. This setup naturally arises in frameworks with multiple axions or braneworld constructions and avoids some of the structural challenges faced by single-field models, while also evading the standard inflationary no-hair arguments that typically erase observable imprints of pre-inflationary or transient dynamics.

A key consequence of such interruptions is the generation of distinctive gravitational wave signals. In models where axion-like inflatons couple to dark $U(1)$ gauge fields, the end of an inflationary stage can trigger exponentially enhanced production of gauge modes, which rapidly source chiral gravitational waves. Unlike the nearly scale-invariant stochastic background expected from vacuum fluctuations, these signals are sharply localized in frequency. Earlier work has shown that interruptions occurring $\mathcal{O}(10)$ efolds before the end of inflation can produce strong gravitational wave backgrounds at subhorizon scales, potentially accessible to current and future experiments.

Focusing on interruptions occurring only a few efolds before the end of the final inflationary stage, we find that the resulting gravitational waves today populate the high-frequency band $f \sim 10^4 - 5 \times 10^5$ Hz, corresponding to wavelengths of order 100 m to tens of kilometers. These frequencies lie in a regime where contamination from late-universe astrophysical and cosmological sources is minimal. Remarkably, the predicted strain can approach the sensitivity thresholds of proposed terrestrial detectors such as the Einstein Telescope, Cosmic Explorer, and Levitated Sensor Detector experiments. Because the signal is extremely narrow in frequency, its total energy density easily satisfies existing bounds from BBN and other gravitational wave constraints, even when the peak amplitude greatly exceeds that of competing sources.

These results identify a qualitatively new observational window on inflationary physics. Multi-stage inflation with brief interruptions can leave pronounced, localized gravitational wave signatures that are both theoretically motivated and experimentally accessible, offering a promising avenue for probing the microphysics of inflation well beyond the reach of conventional cosmological observables.

Acknowledgments: N.K. and A.W. would like to thank “Schweinske” Bahrenfeld for providing a hospitable atmosphere and a free WIFI connection. AG acknowledges support from NSF grants PHY-2409472 and PHY-2111544, DARPA, the John Templeton Foundation, the W.M. Keck Foundation, the Simons Foundation, the Alfred P. Sloan Foundation under Grant No. G-2023-21130, the Gordon and Betty Moore Foundation Grant GBMF12328, DOI 10.37807/GBMF12328. NK is supported in part by the DOE Grant DE-SC0009999. AW is partially supported by the Deutsche Forschungsgemeinschaft under Germany’s Excellence Strategy - EXC 2121 “Quantum Universe” - 390833306, by the Deutsche Forschungsgemeinschaft through a German-Israeli Project Cooperation (DIP) grant “Holography and the Swampland”, and by the Deutsche Forschungsgemeinschaft through the Collaborative Research Center SFB 1624 “Higher Structures, Moduli Spaces, and Integrability”.

References

- [1] A. H. Guth, “The Inflationary Universe: A Possible Solution to the Horizon and Flatness Problems,” *Adv. Ser. Astrophys. Cosmol.* **3** (1987) 139–148.
- [2] A. D. Linde, “A New Inflationary Universe Scenario: A Possible Solution of the Horizon, Flatness, Homogeneity, Isotropy and Primordial Monopole Problems,” *Adv. Ser. Astrophys. Cosmol.* **3** (1987) 149–153.

- [3] A. Albrecht and P. J. Steinhardt, “Cosmology for Grand Unified Theories with Radiatively Induced Symmetry Breaking,” *Adv. Ser. Astrophys. Cosmol.* **3** (1987) 158–161.
- [4] D. H. Lyth, “What would we learn by detecting a gravitational wave signal in the cosmic microwave background anisotropy?,” *Phys. Rev. Lett.* **78** (1997) 1861–1863, [arXiv:hep-ph/9606387](https://arxiv.org/abs/hep-ph/9606387).
- [5] G. Efstathiou and K. J. Mack, “The Lyth Bound Revisited,” *JCAP* **0505** (2005) 008, [arXiv:astro-ph/0503360](https://arxiv.org/abs/astro-ph/0503360).
- [6] N. Kaloper, A. Lawrence, and L. Sorbo, “An Ignoble Approach to Large Field Inflation,” *JCAP* **1103** (2011) 023, [arXiv:1101.0026 \[hep-th\]](https://arxiv.org/abs/1101.0026).
- [7] E. Silverstein, “TASI lectures on cosmological observables and string theory,” in *Theoretical Advanced Study Institute in Elementary Particle Physics: New Frontiers in Fields and Strings*, pp. 545–606. 2017. [arXiv:1606.03640 \[hep-th\]](https://arxiv.org/abs/1606.03640).
- [8] R. M. Wald, “Asymptotic behavior of homogeneous cosmological models in the presence of a positive cosmological constant,” *Phys. Rev. D* **28** (1983) 2118–2120.
- [9] N. Kaloper and J. Scargill, “Quantum Cosmic No-Hair Theorem and Inflation,” *Phys. Rev. D* **99** no. 10, (2019) 103514, [arXiv:1802.09554 \[hep-th\]](https://arxiv.org/abs/1802.09554).
- [10] G. D’Amico and N. Kaloper, “Rollercoaster cosmology,” *JCAP* **08** (2021) 058, [arXiv:2011.09489 \[hep-th\]](https://arxiv.org/abs/2011.09489).
- [11] L. A. Kofman, A. D. Linde, and A. A. Starobinsky, “Inflationary Universe Generated by the Combined Action of a Scalar Field and Gravitational Vacuum Polarization,” *Phys. Lett. B* **157** (1985) 361–367.
- [12] A. A. Starobinsky, “Multicomponent de Sitter (Inflationary) Stages and the Generation of Perturbations,” *JETP Lett.* **42** (1985) 152–155.
- [13] J. Silk and M. S. Turner, “Double Inflation,” *Phys. Rev. D* **35** (1987) 419.
- [14] V. F. Mukhanov and M. I. Zelnikov, “What kinds of perturbation spectra can be produced by inflation?,” *Phys. Lett. B* **263** (1991) 169–175.
- [15] D. Polarski and A. A. Starobinsky, “Spectra of perturbations produced by double inflation with an intermediate matter dominated stage,” *Nucl. Phys. B* **385** (1992) 623–650.
- [16] S. Pi, M. Sasaki, and Y.-l. Zhang, “Primordial Tensor Perturbation in Double Inflationary Scenario with a Break,” *JCAP* **06** (2019) 049, [arXiv:1904.06304 \[gr-qc\]](https://arxiv.org/abs/1904.06304).
- [17] T. Damour and V. F. Mukhanov, “Inflation without slow roll,” *Phys. Rev. Lett.* **80** (1998) 3440–3443, [arXiv:gr-qc/9712061](https://arxiv.org/abs/gr-qc/9712061).

- [18] J. A. Adams, G. G. Ross, and S. Sarkar, “Multiple inflation,” *Nucl. Phys.* **B503** (1997) 405–425, [arXiv:hep-ph/9704286](https://arxiv.org/abs/hep-ph/9704286).
- [19] C. P. Burgess, R. Easther, A. Mazumdar, D. F. Mota, and T. Multamaki, “Multiple inflation, cosmic string networks and the string landscape,” *JHEP* **05** (2005) 067, [arXiv:hep-th/0501125](https://arxiv.org/abs/hep-th/0501125).
- [20] M. Cicoli, S. Downes, B. Dutta, F. G. Pedro, and A. Westphal, “Just enough inflation: power spectrum modifications at large scales,” *JCAP* **12** (2014) 030, [arXiv:1407.1048 \[hep-th\]](https://arxiv.org/abs/1407.1048).
- [21] A. Arvanitaki, S. Dimopoulos, S. Dubovsky, N. Kaloper, and J. March-Russell, “String Axiverse,” *Phys. Rev.* **D81** (2010) 123530, [arXiv:0905.4720 \[hep-th\]](https://arxiv.org/abs/0905.4720).
- [22] G. D’Amico, N. Kaloper, and A. Westphal, “Double Monodromy Inflation: A Gravity Waves Factory for CMB-S4, LiteBIRD and LISA,” *Phys. Rev. D* **104** no. 8, (2021) L081302, [arXiv:2101.05861 \[hep-th\]](https://arxiv.org/abs/2101.05861).
- [23] G. D’Amico, N. Kaloper, and A. Westphal, “General double monodromy inflation,” *Phys. Rev. D* **105** no. 10, (2022) 103527, [arXiv:2112.13861 \[hep-th\]](https://arxiv.org/abs/2112.13861).
- [24] G. Servant and P. Simakachorn, “Ultrahigh frequency primordial gravitational waves beyond the kHz: The case of cosmic strings,” *Phys. Rev. D* **109** no. 10, (2024) 103538, [arXiv:2312.09281 \[hep-ph\]](https://arxiv.org/abs/2312.09281).
- [25] **LIGO Scientific** Collaboration, B. P. Abbott *et al.*, “Exploring the Sensitivity of Next Generation Gravitational Wave Detectors,” *Class. Quant. Grav.* **34** no. 4, (2017) 044001, [arXiv:1607.08697 \[astro-ph.IM\]](https://arxiv.org/abs/1607.08697).
- [26] S. Hild *et al.*, “Sensitivity Studies for Third-Generation Gravitational Wave Observatories,” *Class. Quant. Grav.* **28** (2011) 094013, [arXiv:1012.0908 \[gr-qc\]](https://arxiv.org/abs/1012.0908).
- [27] **LIGO Scientific, Virgo** Collaboration, B. P. Abbott *et al.*, “Search for the isotropic stochastic background using data from Advanced LIGO’s second observing run,” *Phys. Rev. D* **100** no. 6, (2019) 061101, [arXiv:1903.02886 \[gr-qc\]](https://arxiv.org/abs/1903.02886).
- [28] M. Punturo *et al.*, “The Einstein Telescope: A third-generation gravitational wave observatory,” *Class. Quant. Grav.* **27** (2010) 194002.
- [29] **LIGO Scientific, VIRGO** Collaboration, J. Aasi *et al.*, “Characterization of the LIGO detectors during their sixth science run,” *Class. Quant. Grav.* **32** no. 11, (2015) 115012, [arXiv:1410.7764 \[gr-qc\]](https://arxiv.org/abs/1410.7764).
- [30] **LISA Cosmology Working Group** Collaboration, P. Auclair *et al.*, “Cosmology with the Laser Interferometer Space Antenna,” *Living Rev. Rel.* **26** no. 1, (2023) 5, [arXiv:2204.05434 \[astro-ph.CO\]](https://arxiv.org/abs/2204.05434).

[31] N. Aggarwal *et al.*, “Challenges and opportunities of gravitational-wave searches at MHz to GHz frequencies,” *Living Rev. Rel.* **24** no. 1, (2021) 4, [arXiv:2011.12414](https://arxiv.org/abs/2011.12414) [gr-qc].

[32] P. A.-S. et al., “Laser interferometer space antenna,” 2017. <https://arxiv.org/abs/1702.00786>.

[33] K. Yagi and N. Seto, “Detector configuration of DECIGO/BBO and identification of cosmological neutron-star binaries,” *Phys. Rev. D* **83** (2011) 044011, [arXiv:1101.3940](https://arxiv.org/abs/1101.3940) [astro-ph.CO]. [Erratum: Phys. Rev. D 95, 109901 (2017)].

[34] **AEDGE** Collaboration, Y. A. El-Neaj *et al.*, “AEDGE: Atomic Experiment for Dark Matter and Gravity Exploration in Space,” *EPJ Quant. Technol.* **7** (2020) 6, [arXiv:1908.00802](https://arxiv.org/abs/1908.00802) [gr-qc].

[35] **KAGRA, LIGO Scientific, Virgo** Collaboration, B. P. Abbott *et al.*, “Prospects for observing and localizing gravitational-wave transients with Advanced LIGO, Advanced Virgo and KAGRA,” *Living Rev. Rel.* **19** (2016) 1, [arXiv:1304.0670](https://arxiv.org/abs/1304.0670) [gr-qc].

[36] D. Blas and A. C. Jenkins, “Bridging the μ Hz Gap in the Gravitational-Wave Landscape with Binary Resonances,” *Phys. Rev. Lett.* **128** no. 10, (2022) 101103, [arXiv:2107.04601](https://arxiv.org/abs/2107.04601) [astro-ph.CO].

[37] M. A. Fedderke, P. W. Graham, and S. Rajendran, “Asteroids for μ Hz gravitational-wave detection,” *Phys. Rev. D* **105** no. 10, (2022) 103018, [arXiv:2112.11431](https://arxiv.org/abs/2112.11431) [gr-qc].

[38] L. McAllister, E. Silverstein, and A. Westphal, “Gravity Waves and Linear Inflation from Axion Monodromy,” *Phys. Rev. D* **82** (2010) 046003, [arXiv:0808.0706](https://arxiv.org/abs/0808.0706) [hep-th].

[39] N. Kaloper and L. Sorbo, “A Natural Framework for Chaotic Inflation,” *Phys. Rev. Lett.* **102** (2009) 121301, [arXiv:0811.1989](https://arxiv.org/abs/0811.1989) [hep-th].

[40] X. Dong, B. Horn, E. Silverstein, and A. Westphal, “Simple exercises to flatten your potential,” *Phys. Rev. D* **84** (2011) 026011, [arXiv:1011.4521](https://arxiv.org/abs/1011.4521) [hep-th].

[41] N. Kaloper and A. Lawrence, “London equation for monodromy inflation,” *Phys. Rev. D* **95** no. 6, (2017) 063526, [arXiv:1607.06105](https://arxiv.org/abs/1607.06105) [hep-th].

[42] G. Dvali, “Three-form gauging of axion symmetries and gravity,” [arXiv:hep-th/0507215](https://arxiv.org/abs/hep-th/0507215).

[43] G. D’Amico, N. Kaloper, and A. Lawrence, “Monodromy Inflation in the Strong Coupling Regime of the Effective Field Theory,” *Phys. Rev. Lett.* **121** no. 9, (2018) 091301, [arXiv:1709.07014](https://arxiv.org/abs/1709.07014) [hep-th].

[44] M. Dias, J. Frazer, and A. Westphal, “Inflation as an Information Bottleneck - A strategy for identifying universality classes and making robust predictions,” *JHEP* **05** (2019) 065, [arXiv:1810.05199 \[hep-th\]](https://arxiv.org/abs/1810.05199).

[45] B. A. Campbell, N. Kaloper, R. Madden, and K. A. Olive, “Physical properties of four-dimensional superstring gravity black hole solutions,” *Nucl. Phys. B* **399** (1993) 137–168, [arXiv:hep-th/9301129](https://arxiv.org/abs/hep-th/9301129).

[46] M. M. Anber and L. Sorbo, “N-flationary magnetic fields,” *JCAP* **0610** (2006) 018, [arXiv:astro-ph/0606534](https://arxiv.org/abs/astro-ph/0606534).

[47] M. M. Anber and L. Sorbo, “Naturally inflating on steep potentials through electromagnetic dissipation,” *Phys. Rev. D* **81** (2010) 043534, [arXiv:0908.4089 \[hep-th\]](https://arxiv.org/abs/0908.4089).

[48] N. Barnaby, E. Pajer, and M. Peloso, “Gauge Field Production in Axion Inflation: Consequences for Monodromy, non-Gaussianity in the CMB, and Gravitational Waves at Interferometers,” *Phys. Rev. D* **85** (2012) 023525, [arXiv:1110.3327 \[astro-ph.CO\]](https://arxiv.org/abs/1110.3327).

[49] J. L. Cook and L. Sorbo, “Particle production during inflation and gravitational waves detectable by ground-based interferometers,” *Phys. Rev. D* **85** (2012) 023534, [arXiv:1109.0022 \[astro-ph.CO\]](https://arxiv.org/abs/1109.0022). [Erratum: Phys. Rev. D 86, 069901 (2012)].

[50] V. Domcke, F. Muia, M. Pieroni, and L. T. Witkowski, “PBH dark matter from axion inflation,” *JCAP* **07** (2017) 048, [arXiv:1704.03464 \[astro-ph.CO\]](https://arxiv.org/abs/1704.03464).

[51] G. Dall’Agata, S. González-Martín, A. Papageorgiou, and M. Peloso, “Warm dark energy,” *JCAP* **08** (2020) 032, [arXiv:1912.09950 \[hep-th\]](https://arxiv.org/abs/1912.09950).

[52] V. Domcke, V. Guidetti, Y. Welling, and A. Westphal, “Resonant backreaction in axion inflation,” *JCAP* **09** (2020) 009, [arXiv:2002.02952 \[astro-ph.CO\]](https://arxiv.org/abs/2002.02952).

[53] C. Caprini and D. G. Figueroa, “Cosmological Backgrounds of Gravitational Waves,” *Class. Quant. Grav.* **35** no. 16, (2018) 163001, [arXiv:1801.04268 \[astro-ph.CO\]](https://arxiv.org/abs/1801.04268).

[54] **ACT** Collaboration, E. Calabrese *et al.*, “The Atacama Cosmology Telescope: DR6 Constraints on Extended Cosmological Models,” [arXiv:2503.14454 \[astro-ph.CO\]](https://arxiv.org/abs/2503.14454).

[55] **SPT-3G** Collaboration, E. Camphuis *et al.*, “SPT-3G D1: CMB temperature and polarization power spectra and cosmology from 2019 and 2020 observations of the SPT-3G Main field,” [arXiv:2506.20707 \[astro-ph.CO\]](https://arxiv.org/abs/2506.20707).

[56] J. Aasi, B. Abbott, R. Abbott, T. Abbott, M. Abernathy, K. Ackley, C. Adams, T. Adams, P. Addesso, R. Adhikari, *et al.*, “Advanced ligo,” *Classical and quantum gravity* **32** no. 7, (2015) 074001.

[57] J. e. a. Aasi, “Enhanced sensitivity of the ligo gravitational wave detector by using squeezed states of light,” *Nature Photonics* **7** no. 8, (Aug, 2013) 613–619. <https://doi.org/10.1038/nphoton.2013.177>.

[58] A. Arvanitaki and A. A. Geraci, “Detecting high-frequency gravitational waves with optically levitated sensors,” *Phys. Rev. Lett.* **110** (Feb, 2013) 071105. <https://link.aps.org/doi/10.1103/PhysRevLett.110.071105>.

[59] N. Aggarwal, G. P. Winstone, M. Teo, M. Baryakhtar, S. L. Larson, V. Kalogera, and A. A. Geraci, “Searching for new physics with a levitated-sensor-based gravitational-wave detector,” *Phys. Rev. Lett.* **128** (Mar, 2022) 111101. <https://link.aps.org/doi/10.1103/PhysRevLett.128.111101>.

[60] N. Aggarwal, O. D. Aguiar, D. Blas, A. Bauswein, G. Cella, S. Clesse, A. M. Cruise, V. Domcke, S. Ellis, D. G. Figueroa, G. Franciolini, C. Garcia-Cely, A. Geraci, M. Goryachev, H. Grote, M. Hindmarsh, A. Ito, J. Kopp, S. M. Lee, K. Martineau, J. McDonald, F. Muia, N. Mukund, D. Ottaway, M. Peloso, K. Peters, F. Quevedo, A. Ricciardone, A. Ringwald, J. Steinlechner, S. Steinlechner, S. Sun, C. Tamarit, M. E. Tobar, F. Torrenti, C. Ünal, and G. White, “Challenges and opportunities of gravitational wave searches above 10 khz,” 2025. <https://arxiv.org/abs/2501.11723>.

[61] **LSD Collaboration** Collaboration, G. Winstone, Z. Wang, S. Klomp, R. G. Felsted, A. Laeuger, C. Gupta, D. Grass, N. Aggarwal, J. Sprague, P. J. Pauzauskie, S. L. Larson, V. Kalogera, and A. A. Geraci, “Optical trapping of high-aspect-ratio nayf hexagonal prisms for khz-mhz gravitational wave detectors,” *Phys. Rev. Lett.* **129** (Jul, 2022) 053604. <https://link.aps.org/doi/10.1103/PhysRevLett.129.053604>.

[62] V. Jain, J. Gieseler, C. Moritz, C. Dellago, R. Quidant, and L. Novotny, “Direct measurement of photon recoil from a levitated nanoparticle,” *Phys. Rev. Lett.* **116** (Jun, 2016) 243601. <https://link.aps.org/doi/10.1103/PhysRevLett.116.243601>.

[63] A. Derevianko, “Detecting dark-matter waves with a network of precision-measurement tools,” *Phys. Rev. A* **97** (Apr, 2018) 042506. <https://link.aps.org/doi/10.1103/PhysRevA.97.042506>.